Title: Multisite imaging of neural activity using a genetically encoded calcium sensor in the honey bee *Apis mellifera*

Short title: Neural recordings using transgenic honey bees

Authors: Julie Carcaud[1*], Marianne Otte[2], Bernd Grünewald[3], Albrecht Haase[4,5,6], Jean-Christophe Sandoz[1,6], Martin Beye[2,6]

*Corresponding author: Julie Carcaud, Evolution, Genomes, Behavior and Ecology, Université Paris-Saclay, CNRS, IRD, Gif-sur-Yvette, France. Email: julie.carcaud@egce.cnrs-gif.fr. Phone: +33169823752

Author's addresses:

[1] Evolution, Genomes, Behavior and Ecology, Université Paris-Saclay, CNRS, IRD, Gif-sur-Yvette, France

[2] Evolutionnary Genetics, Heinrich Heine University Düsseldorf, Düsseldorf, Germany

[3]Institut für Bienenkunde, Polytechnische Gesellschaft, FB Biowissenschaften, Goethe-University, Frankfurt am Main, Germany

[4] Center for Mind/Brain Sciences, University of Trento, Rovereto, Italy

[5] Department of Physics, University of Trento, Trento, Italy

[6]These authors jointly supervised this work

ABSTRACT

Sociality is classified as one of the major transitions in evolution, and the most advanced level of sociality is found in eusocial insects such as the honey bees. This sophisticated social behavior seems to be associated with higher cognitive abilities in these insects, however the study of their neural bases has been limited by the lack of tools that allow measuring neuronal activity simultaneously in different brain regions of the honey bee brain. Here, we developed the first pan-neuronal genetic driver in a Hymenopteran model organism, the honey bee, and expressed the calcium indicator GCaMP6f under the control of the honey bee *synapsin* promoter. We show that GCaMP6f is widely expressed in the honey bee brain, allowing to record neural activity from multiple brain regions simultaneously, including from poorly investigated brain regions such as the mushroom body calyces or the lateral horn. Our recordings show that while odorant quality (chemical structure) and quantity are faithfully encoded in the honeybee antennal lobe, odor coding in the lateral horn departs from this simple physico-chemical coding, in line with the role of this structure in coding the biological value of odorants. These brain recordings represent the first use of a neurogenetic tool for recording neural activity in a eusocial insect.

Keywords: Insect, brain, olfaction, transgenesis, calcium imaging, GCaMP

INTRODUCTION

Sociality is classified as one of the major transitions in evolution, and animals often form social groups because the benefits of grouping (either direct or indirect) outweigh the costs of breeding independently (1, 2). The most advanced level of sociality is found in eusocial insect societies (3, 4), and the insect order Hymenoptera (including ants, bees and wasps) presents the largest number of eusocial species. Among them, honey bees are a classical model for the study of eusocial behavior, as they live in colonies composed of up to 60,000 individuals, consisting of three adult castes (queen, worker, and male). Within the worker caste, honey bees show a clear division of labor with a specialization of roles (5). The success of honey bee colonies lies in the capacity of all members of the society to behave in a well-organized and context-dependent manner, a social behavior mediated in part by olfactory cues such as pheromones used for communication among the colony (6).

Previous research found that this sophisticated social behavior is associated with higher cognitive abilities in these insects, and in this context, honey bees is a mainstream model for studying higher-order insect cognition such as navigation (7), rule learning (8), social learning (9), dance communication(10) but also olfactory perception and learning (11-13). However, whether the evolutionary rise of these sophisticated social behaviors is associated with the formation of specific neuronal pathways and structures has not been sufficiently resolved (14, 15). Progress in understanding these sophisticated behaviors and how social cues are processed and integrated with higher order cognitive abilities have in part been limited due to the lack of tools allowing to measure neuronal activity simultaneously in different regions of the honey bee brain.

For now, honey bee neuroscience remains limited to the use of conventional neuroanatomy (16), pharmacology (17), electrophysiology (18), and imaging tools (13, 19). However, the development of neurogenetic tools during the 20th century has provided unprecedented progress in our understanding of the neural basis of behavior in other model species. Among others, this approach allowed to decipher the brain circuits underlying aggressive behavior (20), courtship (21), or memory

79 (22) in a limited set of model species, both vertebrates such as mouse or zebrafish and invertebrates.
80 In insects, the fruit fly *Drosophila melanogaster* has been for many years the leading model for
81 investigating the neural basis of behavior, from gene expression to neural circuits (23-25). Recently,
82 neurogenetic approaches have been developed in other Diptera such as mosquitoes (26, 27) and in
83 some Lepidoptera (28, 29) to understand specific behaviors such as human-host seeking (30, 31) or
84 insect-plant interactions (32), mainly focusing on their olfactory capabilities. However, genetic
85 methods are particularly difficult to apply in eusocial insects, since genetic transformation rates are
86 low, endogenous promotors for neuronal expressions are unknown and the genetically manipulated,
87 reproductive individuals (the queens) have to be maintained in larger colonies with workers in
88 containments (33).

89 Despite the difficulty, the recent use of the genome editing tool CRISPR/Cas9 in the honey bee
90 allowed to knock out specific genes, such as the sex-determining *dsx* gene (34), the olfactory co-
91 receptor gene *orco* (35), the gustatory receptor *AmGr3* gene (36) or the *Amyellow-y* gene (37). Even if
92 these studies evaluated the effect of specific mutations at the neuronal (35) or the behavioral levels
93 (36), versatile genetic tools allowing to investigate the neural basis of a wide range of higher-order
94 social behaviors and learning in honey bees are still missing. The advent of genetically-encoded neural
95 activity sensors, in particular calcium sensors, has represented a major breakthrough in *Drosophila* or
96 mouse research (38-40), but such a critical tool for circuit dissection is still lacking in Hymenoptera.

97 To this aim, we developed the first pan-neuronal genetic driver in a Hymenopteran model
98 organism, the honey bee, and expressed the calcium indicator GCaMP6f under the control of the honey
99 bee *synapsin* promoter. We characterized its expression pattern in the honey bee brain and evaluated
100 its potential as a functional tool by recording neural activity upon olfactory stimulation. We show that
101 GCaMP6f expression allows to record olfactory responses from multiple brain regions simultaneously,
102 after simply opening the brain capsule. By using a controlled panel of well-characterized odorants, we
103 show that the recorded signals reveal robust odor coding rules. This new pan-neuronal genetic driver
104 also permits to record neural activity from poorly recorded regions of the brain such as the lateral horn

105 and the mushroom body calyces, and allowed to find that olfactory chemical features are less
106 represented in the lateral horn than in the antennal lobe. This study opens extraordinary new
107 possibilities for neuroethological research in the honey bee to study the neural basis of advanced social
108 behaviors and cognitive skills.
109
110
111 **RESULTS**
112 This work aimed at expressing the calcium-sensitive protein GCaMP6f in a pan-neuronal manner in the
113 honey bee brain to record neural activity in this social insect.
114
115 **Generation of transgenic honey bees**
116 In order to generate a bee with a possibly pan-neuronally expressed calcium sensor, we introduced a
117 synapsin (syn) promoter GCaMP6f expression cassette (*syn-GCaMP6f*) into the genome using the
118 *piggyBac* (PB) transposon system (33). To generate this *syn-GCaMP6f* expression cassette we cloned
119 the 1 kb promoter region together with the entire 5' untranslated region (5' UTR) of the *synapsin* gene
120 from the honey bee, which we then fused with the coding sequence of the GCaMP6f sensor protein
121 (Figure 1 A). We obtained a transgenic *syn-GCaMP6f* queen using previously published procedures and
122 a hyperactive transposase (33, 41). We instrumentally inseminated the queen and reared from the
123 offspring 2nd generation queens. Only 1% of those queens were carrying the transgene, which we
124 identified from transgene amplifications. The 2nd generation *syn-GCaMP6f* queens produced 50% *syn-*
125 *GCaMP6f* worker offspring bees, which we used in the neuroanatomy and imaging experiments.
126
127 **Pattern expression of the GCaMP6f in the brain**
128 We first studied the pattern expression of GCaMP6f in the brain using immunostaining against
129 GFP (Figure 1B-C), the green fluorescent protein which the GCaMP6f sensor contains. We found clear
130 and widespread staining throughout the brain, with strong staining in the antennal lobes (ALs), the

131 optic lobes (OLs), and the mushroom bodies (MBs) suggesting that the GCaMP6f protein is ubiquitously
132 expressed in all major brain structures. Within neurons, we found evidence of staining in somata
133 (Figure 1B left, white arrows) as well as neuronal processes (see for instance neural tracts around the
134 α-lobe; Figure 1B left, white arrows). At the level of the AL (Figure 1C left), lateral and medial clusters
135 of projection neurons and local interneurons somata show strong GCaMP6f immunostaining. In
136 addition, glomeruli seem homogeneously stained: staining in the cortex suggests expression in
137 olfactory sensory neurons (OSNs) terminal projections, whereas staining in the glomerulus core
138 suggests expression in projection neurons (PNs) dendrites and possibly local neurons. Finally, the
139 clearest expression of GCaMP6f was found in somata at the level of the calyces of the MB (Figure 1C
140 right). In these structures, different neuron types are stained, with somata of class I Kenyon Cells in
141 the cup-shaped calyces and class II Kenyon Cell somata lying outside the calyces (see white arrow in
142 Figure 1C right) (42, 43).

143 We next asked whether the cloned synapsin promoter used for GCaMP6f expression drives the
144 same expression pattern as the one of the *synapsin* gene. To answer this question, we performed a
145 complementary immunostaining targeting the synapsin protein (Figure 1B right, anti-SYNORF1 in red).
146 We found co-localized staining of GCaMP6f and synapsin within AL glomeruli both in the cortex and
147 the core (Figure 1C), demonstrating co-expression within AL neurons. This experiment also shows
148 differences between GCaMP6f and synapsin stainings. The synapsin immunostaining allows to clearly
149 visualize presynaptic zones, for instance in AL glomeruli or microglomeruli in the MB calyces, but is not
150 present in the somata unlike GCaMP6f. This result indicates that even if GCaMP6f is expressed in cells
151 expressing synapsin (in theory all neurons), these 2 proteins appear to be partially differently localized
152 within neurons.

153 We conclude that GCaMP6f was widely expressed in the honey bee brain, one of the
154 prerequisites for whole-brain functional recordings of neural activity.

155

156

157 **Calcium imaging**

158 *Neural recordings in the whole brain*

159 GCaMP6f expression in neurons was then used to record neural activity in the honey bee brain (Figure
160 2). As a proof of concept for the use of these bees in neuroethological research, we decided to focus
161 here on olfactory information processing, as olfaction is the best understood sensory modality in honey
162 bees. Right after placing the bee in a recording chamber and opening its head capsule, we first
163 presented a few standard odorants while recording the whole brain surface accessible under the
164 microscope objective. Odorant presentations triggered a clear GCaMP fluorescence change from
165 several brain regions, including the primary olfactory centers (the antennal lobes, ALs) and both higher-
166 order centers (the lateral horns, LHs and the mushroom bodies, MBs), known for their role in olfactory
167 processing (Figure 2A). The use of GCaMP-expressing bees allowed us to record neural activity
168 simultaneously in all these structures (Figure 2B), while the presentation of an unscented air control
169 did not induce such activity. Response amplitudes were stronger in the AL (Figure 2C left) than in the
170 LH (Figure 2C middle) or in the MB (Figure 2C right). In all regions, the recorded calcium signals showed
171 a biphasic response, with a fluorescence increase upon odor presentation followed by a long
172 undershoot. Such biphasic signals are reminiscent of calcium signals previously recorded using bath-
173 applied calcium-sensitive dyes (44, 45). This experiment represents the first recording of neural activity
174 using neurogenetic tools outside of Diptera.

175

176 *Neural recordings in the antennal lobe (AL)*

177 We then asked if the signals recorded using this genetically-encoded calcium sensor represent
178 neural signals that are meaningful in terms of sensory coding, focusing first on the primary olfactory
179 center, the antennal lobe (AL), since olfactory coding was best studied in this structure. To this aim,
180 we presented 16 aliphatic odorants used in previous imaging studies either after bath-application of a
181 cell-permeant calcium-sensitive dye (Calcium-green 2-AM, OSN recordings) (45) or after insertion of a
182 migrating calcium-sensitive dye within a neural tract (Fura-2 dextran, PN recordings) (19). The

183 response patterns to the 16 aliphatic odors differed systematically according to their functional group
184 (primary or secondary alcohols, aldehydes, or ketones) or their carbon chain length (from 6 to 9
185 carbons). As observed with other calcium reporters, the presentation of each odorant induced a
186 biphasic signal in a different set of AL glomeruli while presentation of the air control did not induce
187 such response (Figure 3A-B). The averaged AL response amplitudes were significantly different from
188 the air control for all 16 odors (Figure 3C, RM-ANOVA, odor effect $F_{16,160} = 12.49$, p = 8e-21, post hoc
189 Dunnett tests $p < 0.0097$). Signal amplitudes differed according to the odor (odor effect, p = 8e-21),
190 and were related to the quantity of molecules in headspace, since odor-evoked responses were highly
191 correlated with the vapor pressure of the odorants (Figure 3D, $R^2 = 0.84$, Fisher test $F_{1,14} = 73.72$, p =
192 6e-7). Such a correlation was also found in previous studies recording at AL input (OSNs)(45) or output
193 (PNs)(19). This strong dependence explains why odor-evoked intensities recorded using genetically
194 encoded GCaMP6f in this study are highly correlated with odor-evoked intensities recorded in OSNs
195 (Sup. Figure 1A, $R^2 = 0.84$, $F_{1,14} = 74.23$, p = 6e-7) or in PNs (Sup. Figure 1B, $R^2 = 0.78$, $F_{1,14} = 49.73$, p =
196 6e-6).

197 We then evaluated odor coding in the GCaMP bees by comparing similarity relationships
198 among odorants, by calculating Euclidian distances between response maps obtained for the different
199 odor pairs. First, we confirmed that within each bee, each odorant evokes a specific activity pattern,
200 as distances were lower for different presentations of the same odorant than for the presentation of
201 different odorants (Figure 3E, paired t-test $t = 6.15$, p = 1.08e-4). This result fits with previous calcium
202 imaging data both at AL input and output (46, 47). We then performed a hierarchical cluster analysis
203 using Euclidian distances between odorants. We found a first segregation between odorants with long
204 chain lengths and odorants with short chain lengths (Figure 3F, C6-C7 vs. C8-C9). Within the shorter
205 chain length group, a further separation between functional groups appeared based on the oxygen
206 moiety (C=O for aldehydes and ketones vs. C-OH for alcohols). Within the longer chain length group,
207 aldehydes were separated from the other odorants. This analysis shows a clear coding depending on
208 the chemical structure of the odorants, and with remarkably similar results as in previous studies using

209 non-transgenic approaches (19, 45). Accordingly, inter-odorant distances found in the GCaMP bees
210 were highly significantly correlated with those measured previously in OSNs using calcium dye bath
211 application (R^2 = 0.53, Mantel test p = 1.0e-4) or measured in PNs using dye injection (R^2 = 0.44, Mantel
212 test p = 1.0e-4). The correlation coefficients were not significantly different (R^2 = 0.53 vs. R^2 = 0.44, z =
213 0.98, p = 0.33, NS), suggesting the possibility that both OSN and PN contribute to the signals recorded
214 in the AL using genetically encoded GCaMP6f.

215 Finally, we asked if odorant response maps recorded with the GCaMP bees relate to bees'
216 actual perception of the odorants. We thus correlated the Euclidian distances measured between all
217 odor pairs in this study with distances measured in an appetitive conditioning experiment(48). We
218 found that behavioral distances can be predicted using signals recorded with genetically encoded
219 GCaMP6f (data not shown; R^2 = 0.34, Mantel test p = 1.0e-4). Thus, odorants evoking similar activity
220 patterns in the AL are treated as similar by honey bees in their behavior, a further confirmation that
221 GCaMP6f expression allows to record meaningful neural signals.

222

223 *Neural recordings in the lateral horn (LH)*

224 We then studied olfactory information processing in higher-order brain centers, first focusing
225 on the LH. All the aliphatic odorants used in this panel induced calcium signals in the LH (Figure 4A).
226 Odor-evoked signals systematically followed a biphasic time course, like that recorded in the AL (Figure
227 4B). In the LH, all but one of the presented odorants induced a response that was significantly higher
228 than to the air control (RM-ANOVA, odor effect $F_{16,112}$ = 8.091, p = 0.0014, post hoc Dunnett tests, p <
229 0.04 except p = 0.09 for 2-hexanol). As in the AL, response amplitudes correlated with odorants' vapor
230 pressures (R^2 = 0.49, $F_{1,14}$ = 13.87, p = 0.0023). However, this correlation appeared to be weaker in the
231 LH with a near-significant difference between the two correlation coefficients (R^2 = 0.84 in the AL vs.
232 R^2 = 0.49 in the LH, z = 1.76, p = 0.078). In other words, response intensity in the LH was not a simple
233 product of the number of volatile molecules in the odor puff, possibly revealing a yet undocumented
234 gain control mechanism in the LH.

235 We then compared similarity relationships (Euclidian distances among odorants) measured in
236 the LH and in the AL and found a weak but still significant correlation (R^2 = 0.07, Mantel test p = 0.023).
237 This suggests a transformation of odor similarity relationships between the two structures. A cluster
238 analysis performed on Euclidian distances in the LH confirmed this finding. The analysis roughly
239 segregated alcohols (-OH moiety) on the one side and aldehydes/ketones (=O moiety) on the other.
240 However, different rules apply here, as the two longest chain molecules nonanal and 2-nonanone
241 clustered with the former group, while the shortest chain secondary alcohols, 2-hexanol and 2
242 heptanol clustered with the latter group. Thus, the study of odor coding in the LH using GCaMP bees
243 suggests less clearly dependence on chemical features than in the AL.
244 Nevertheless, Euclidian distances measured in the LH correlated significantly with behavioral
245 distances measures (48) (data not shown; R^2 = 0.12, Mantel test p = 0.0021), demonstrating that
246 odorants evoking similar activity patterns in the LH are treated as similar by honey bees in their
247 behavior.
248
249 *Neural recordings in the mushroom bodies (MB)*
250 Lastly, we turned to the second higher-order center, the mushroom bodies (Figure 5), a
251 multisensory integration center in the honey bee brain. Calcium signals upon odorant presentation
252 were observed at the level of the calyx lip. Calcium signals systematically showed a biphasic time
253 course (Figure 5B) like that recorded in the AL and in the LH, but in all cases with a small first
254 component and a much stronger second component. In this structure, the five presented odorants
255 induced significant activity in the MB calyx in comparison to the air control (Figure 5C; RM-ANOVA,
256 odor effect $F_{5,25}$ = 7.99, p = 0.0033, post hoc Dunnett tests $p < 0.05$, except 2-heptanone with p = 0.07).
257 However, signal-to-noise ratio was considered too low for further analysis of inter-odor relationships.
258
259
260

261 **DISCUSSION**

262 We developed a line of honey bees with pan-neural expression of a genetically-encoded
263 calcium sensor allowing to record neural activity from honey bee neurons. To our knowledge, this
264 represents the first neurogenetic tool for recording neural activity in a non-dipteran insect and eusocial
265 insect. Neurogenetic tools, especially the use of genetically-encoded calcium indicators (GECIs), have
266 been widely developed in both vertebrates (40, 49) and invertebrates (50) and supported major
267 progress in our understanding of the neural basis of behavior. In insects, such possibility was limited
268 until now to a few Dipteran species (fruit flies and mosquitoes (26)) and was lacking in other insects
269 with different lifestyles. The present development in a social Hymenoptera represents a major
270 progress for the neuroethology of social behavior but also a significant achievement in a species like
271 honey bees in which neurogenetic tools are difficult to establish due to its peculiar reproductive
272 biology and the lack of knowledge of appropriate promoter sequences driving the expressions.

273 To develop our pan-neuronal calcium indicator, we expressed GCaMP6f under the control of
274 the promoter of the gene coding for synapsin, a vesicle–associated presynaptic protein found
275 throughout the honey bee brain (51). This strategy was successful, as honey bees displayed broad
276 labeling with GCaMP6f in the major brain structures of the nervous system at sufficient amounts for
277 performing calcium imaging. Our neuroanatomical data confirm significant expression throughout the
278 bee brain (optic lobes, antennal lobe, mushroom bodies, all other regions of the protocerebrum), but
279 we noticed substantial cell-to-cell variation in some regions, for instance in the cup of the mushroom
280 body calyx, which contains the somata of type I Kenyon cells (see Figure 1C): there, a strong contrast
281 appeared among neurons, suggesting differences in the level of GCaMP expression among Kenyon cells
282 or even some Kenyon cells lacking GCaMP expression. The GCaMP staining pattern did not correspond
283 to any of the Kenyon cell subtypes previously described based on their differing gene expression
284 profiles (52). In contrast to the synapsin protein, GCaMP6f is located in the entire neuron, since we
285 detected staining in the somata (Figure 1C), the neurites, and the synaptic regions. This widespread
286 expression could represent a great advantage for performing functional recordings in the bee brain.

287 To assess the power of this new tool for studying brain activity, we focused on the olfactory
288 system, which is the best-known sensory system in this animal. We compared the results obtained
289 using the GCaMP6f bees with previous results acquired using conventional dye injections or bath-
290 application (19, 45). For the first time, we could observe the simultaneous activation of the three main
291 brain structures involved in insect olfaction, the antennal lobe, the lateral horn, and the mushroom
292 body calyx. The possibility to record from these structures at the same time is a first and important
293 step towards the long-term goal to understand brain circuits responsible for bees' sophisticated social
294 behaviors and cognitive abilities, that may unravel yet undescribed sensory and/or behavior-related
295 pathways.

296 To follow this, we first validated our tool using individual structures and we confirmed its
297 validity for measuring relevant neural activity with regard to bees' behavior. Recordings obtained using
298 the GCaMP6f-expressing honey bees revealed the same olfactory coding rules in the AL as in previous
299 studies (19, 53). Thus, odor-induced activity followed the same intensity rule (depending on odorant
300 vapor pressure – Figure 3D) and inter-odorant neural distance measures were organized according to
301 odorants' chemical features, chain length, and functional group. Accordingly, calcium imaging
302 measured with the GCaMP-expressing bees allowed to predict how similarly honey bees perceive these
303 odorants, since inter-odor relationships among GCaMP response maps correlated with inter-odor
304 behavioral distances previously measured in an associative conditioning experiment (48). This result,
305 even if limited to a single sensory modality, is a strong confirmation of the biological pertinence of the
306 signals measured with this new neurogenetic tool.

307 In order to demonstrate that the activity can be followed to higher-order brain structures, we
308 studied the role of the lateral horn in encoding the chemical features of our odorants. The lateral horn
309 is a poorly studied structure in Hymenoptera, which could only be recorded previously using invasive
310 dye injection (54). Importantly, while previous recordings only measured from a limited subpopulation
311 of projection neurons in this structure (the l-ALT), the GCaMP6f-expressing honey bees allowed
312 recording from the whole structure. The recordings in response to the 16 aliphatic odorants showed

313 that odor coding in this higher-order center is less clearly influenced by odorant quantity (*i.e.* lower
314 response amplitude differences among odorants) or by the chemical structure of the odorants than in
315 the AL. These first results suggest the existence of an additional gain control mechanism in this
316 structure, fitting with current discussions on its role in *Drosophila* (55, 56) and the possible coding of
317 hedonic odorant valence rather than chemical features using this new tool.

318 Calcium signals were also recorded in the mushroom body calyx, and odorants clearly activated
319 the lip, the olfactory input region of the calyx, as observed previously with a bath-applied dye (57). The
320 signal amplitude was generally low, which reproduces the known sparseness of the MB odor code (58).
321 Together with the random arrangement of PN terminals and KC dendritic arbors in the lip, this
322 prevented the observation of odor-specific response maps at this point. However, advanced 3D
323 microscopy techniques (59) will benefit from this neurogenetic marker to unravel coding mechanisms
324 also in this neuropil, as experiments in Drosophila promise (60).

325 We expect that recording neuronal activity simultaneously and in detail in brain structures
326 using a genetically expressed Ca reporter in a eusocial insect, the honeybee, as demonstrated here,
327 will open new possibilities to decipher the neural bases of the sophisticated social behavior and its
328 associations with higher cognitive abilities. It will also allow the study of other sensory modalities than
329 the most commonly studied olfaction and vision. As discussed above, this new development enables
330 to record neural activity in different regions of the brain at the same time, which could become a major
331 advantage over non-transgenic approaches, as it allows to reveal a whole neural circuit underlying a
332 specific behavior. Moreover, the study of mechanosensory information processing notably used during
333 the waggle dance remains limited(61, 62) and should be facilitated using GCaMP-expressing honey
334 bees. Lastly, transgenic bees could be instrumental for studying neural signals in response to
335 multisensory inputs, for instance in the mushroom bodies, the higher-order center known for its role
336 in multimodal sensory integration(63).

337 The future of insect neuroethology beyond the use of model organisms like *Drosophila* will
338 depend on the further development of neurogenetic tools in species like honeybees, with their rich

339 behavioral repertoire involving intricate social behaviors as well as elaborated cognitive skills. First, a
340 better resolution will have to be achieved using cell-type-specific gene expression to visualize (*i.e.* using
341 fluorescent proteins such as GFP) or monitor activity (using GECIs as here) from specific neuronal
342 populations. The same precision shall then be exploited to specifically silence or activate specific
343 neuron populations, allowing a temporal control of neural function. We hope that the new line of
344 GCaMP-expressing bees will represent the first step in this direction.
345
346
347 **MATERIAL AND METHODS**
348
349 ***Piggy-Bac* transgenesis**
350 The promoter region together with the three exons of the 5' UTR of the honey bee *synapsin* (*syn*) gene
351 (LOC551737; assembly Amel_4.5) were successively cloned (Sup. Figure 2). This single fragment (1811
352 bp) was inserted into the PBac plasmid(33) using the *Asc*I/*Nco*I restriction sites. The coding sequence
353 of *GCaMP6f* was inserted downstream of the promoter region using *Nco*I/*Mss*I restriction sites that
354 finally resulted in the PBac [*syn-GCaMP6F*] plasmid. Egg injections, larvae and queen rearing were
355 performed following standard methodology by employing the hyperactive transposase which we have
356 customized for the honey bee (33, 41). A total of 4231 honey bee eggs not older than 1.5 h were
357 injected and the hatched larvae were reared to queens. Semen from wildtype drones was used for
358 instrumental insemination of queens. Inseminated queens were laying fertilized, usually female-
359 determined eggs that were reared either to queens or worker bees. Transgenic queens were identified
360 by amplification of the transgene in the offspring(41) using oligonucleotide primers
361 (CCACACCTCCCCCTGAACCTGAAAC and GAGGTAAGAATAAACATTGTTGGTC) targeting the PBac
362 sequence.
363
364 **Anatomical immunostaining**

365 To visualize the expression pattern of the GCaMP6f in the honey bee brain, transgenic workers
366 were caught at emergence and were maintained in an incubator in the dark at 34°C for 2 weeks (*i.e.*
367 the same age as for calcium imaging). The brains of workers were dissected and immediately immersed
368 in cold 1% zinc formaldehyde in PBS (ZnFa 1%(64)) and kept overnight at 4°C. Brains were then washed
369 six times in PBS (10 min each), permeabilized in PBS containing 1% Triton X-100 for 30 min, and pre-
370 incubated 3h in PBS containing 0.3% Triton and 1% BSA (Bovine Serum Albumine in PBS, #37525,
371 ThermoScientific). To stain *GCaMP6f* and *synapsin* (as background staining), the brains were then
372 incubated in PBS containing 0.3% Triton and 0.1% BSA with rabbit polyclonal anti-GFP (Thermofisher,
373 #A-11122, France) at 1:100 dilution and mouse monoclonal anti-SYNORF1 (DHSB, #3C11, US) at 1:100
374 dilution for 7 days. Brains were then washed 6 times in PBS containing 0.3% Triton and incubated in
375 secondary antibodies directed against rabbit coupled to Alexa 488 (Thermofisher, #A11122, France)
376 and against mouse coupled to Alexa 555 (Thermofisher, #A-21147, France) both diluted at 1:200 for 5
377 days. Brains were then washed in PBS, dehydrated in an ascending ethanol series (30% to 100%),
378 cleared, and finally mounted in methyl salicylate (M6752, Sigma-Aldrich, France) for observation.
379 Brains were scanned using a laser-scanning confocal microscope (Zeiss LSM 700) with a W Plan-
380 Apochromat 20x/NA 1 objective using sequential excitation wavelengths of 488 nm and 555 nm,
381 observing via two color-filtered channels around 510 nm and 590 nm, respectively.
382
383 **Honey bee preparation for *in vivo* calcium imaging**
384 Transgenic workers were collected at emergence and were maintained in small cages in the
385 dark at 34°C for 2 weeks. On the day of the experiment, they were individually chilled on ice for 5 min
386 until they stopped moving. Then, they were prepared following the standard preparation used to
387 image the ventral part of the honey bee brain(13, 19, 44, 47). Briefly, the honey bee was fixed in a
388 plastic chamber with its antennae oriented to the front and the proboscis was fixed using beeswax to
389 avoid movement of the brain during the experiment. A pool was built with beeswax and pieces of
390 plastic around the head capsule, and a small window was then cut in the head cuticle. Glands as well

391 as trachea were removed to expose the brain, and the pool was filled with ringer solution (in mM:
392 NaCl, 130; KCl, 6; $MgCl_2$, 4; $CaCl_2$, 5; sucrose, 160; glucose, 25; Hepes, 10; pH 6.7, 500 mOsmol; all
393 chemicals from Sigma-Aldrich, France), to avoid desiccation of the brain surface. The honey bee was
394 then left 30 min in a moisturized and dark place before the calcium imaging.
395
396 **Calcium imaging**
397 A T.I.L.L. Photonics imaging system (Martinsried, Germany) was used to perform *in vivo* optical
398 recordings, as described elsewhere(19, 65). An epifluorescence microscope (Olympus BX51WI) was
399 used to record activity in the different regions of the brain with either a 4× dry objective (Olympus,
400 PlanCN; NA 0.10) for whole-brain recordings, a 10× water-immersion objective (Olympus, UMPlanFL;
401 NA 0.3) for AL recordings or a 20x water-immersion objective (Olympus, UMPlanFL; NA 0.5) for LH and
402 MB recordings. GCaMP6f was excited using 475 nm monochromatic light (T.I.L.L. Polychrom IV). The
403 fluorescence signal was separated by a 505 nm dichroic filter and a long-pass 515 nm emission filter
404 and recorded with a 640 × 480 pixels 12-bit monochrome CCD camera (T.I.L.L. Imago) cooled to -12°C
405 with 4 × 4 binning on chip. Each measurement consisted of 100 frames recorded at a rate of 5 Hz
406 (integration time for each frame ~50ms).
407
408
409 **Odor stimuli**
410 A constant airstream was directed from a distance of 1 cm to the bee's antennae, and odor
411 stimuli were given at the 15th frame for 1 s. For each odor stimulus (all obtained from Sigma-Aldrich,
412 France), 5 µL of the solution were deposited on a filter paper inserted in a Pasteur pipette. A pipette
413 containing a clean piece of filter paper was used as control stimulus.
414 For whole-brain recordings, we tested a small set of 3 odorant stimuli known from previous
415 work to trigger strong neural activity: 2-heptanone, octanal, and heptanal. For AL and LH recordings,
416 we tested 16 aliphatic odorants previously used in calcium imaging studies (19, 45) belonging to 4

417 functional groups (primary and secondary alcohols, aldehydes, and ketones) and having 4 different
418 carbon chain lengths (6, 7, 8, and 9 carbons). The use of these odorants which are part of floral blends
419 honey bees encounter while foraging (Knudsen et al. 1993) allowed to compare the results obtained
420 in this study using GCaMP6f imaging with previous studies using classical calcium-sensitive dyes such
421 as Fura-2 dextran(19) or Calcium green 2-AM(45). These 16 odorants were used to record neural
422 activity at the level of the AL and at the level of the LH on two different groups of bees. For recordings
423 at the level of the MB, a reduced list of odorants which give strong neural activity were used: 1-hexanol,
424 2-hexanone, 2-heptanone, heptanal, octanal, and the air control.
425 Each odorant stimulus was presented twice in a pseudo-randomized order, avoiding the
426 consecutive presentation of stimuli with the same functional group or the same carbon chain length.
427
428 **Data processing and analyses**
429 All analyses were carried out using custom-made software written in IDL 6.0 (Research
430 Systems, Boulder, CO). Each odor presentation corresponded to a three-dimensional array consisting
431 of two spatial dimensions (*x*- and *y*-coordinates) along time (100 frames). First, the relative
432 fluorescence changes were calculated as $\Delta F/F = (F - F_0)/F_0$ by taking as reference background F_0 the
433 average of three frames just before the odorant stimulation (frames 9-11). Possible irregularities of
434 lamp illumination and bleaching were corrected by subtracting the median pixel value of each frame
435 from every single pixel of the corresponding frame. Finally, the two spatial dimensions were filtered
436 with a Gaussian filter of window size 7×7 pixels for AL recordings or 3×3 pixels for LH and MB recordings
437 for noise reduction. A biphasic calcium signal was observed in all recordings. As in previous studies
438 using bath-applied Calcium Green(45), a high contrast measure for the intensity of the odor-induced
439 response was obtained by averaging three consecutive frames at the end of the odor presentation
440 (frames 19-21) and subtracting the average of 3 frames during the second, negative component of the
441 signal (frames 49-51).

442 For the quantification of response intensity and similarity relationships, a mask was precisely
443 drawn in order to exclude regions outside of the imaged structure. A pixel-wise analysis was then
444 performed, using all the pixels within the mask. Response intensity was calculated by averaging the
445 intensity of all pixels located within the unmasked area. Similarity relationships between neural activity
446 patterns $I(x, y)$ were calculated by measuring Euclidian distances

447 $$d(o_1, o_2) = \sqrt{\sum_{x,y} (I_{o_1}(x, y) - I_{o_2}(x, y))^2}$$

448 for all the 120 odorant pairs o_1, o_2 within each animal.

449 For all analyses, average values for the two presentations of each odorant were used except
450 for the comparison of Euclidian distances for the same vs. different odorants (Figure 3E) in which each
451 single odorant presentation was used.

452 We used the Euclidian distances between odorants calculated using behavioral experiments
453 by Guerrieri et al.(48) to compare similarity relationships among odorants at the neural level with data
454 obtained at the behavioral level. All results are displayed as means over individuals ± SEM.

455

456 **Statistical analyses**

457 Odor response intensities were compared with ANOVA for repeated measurements, using
458 odors as within-group factors. A Dunnett post hoc test was applied to compare the intensity of the
459 response to each stimulus with a common reference, the air control. Wilcoxon matched-pairs tests
460 were applied to compare Euclidian distances between the same and different odors for AL recordings.
461 Pearson correlation analyses were performed between response intensity and the logarithm of
462 odorants' vapor pressure in mmHg (16 aliphatic odors recorded in the AL and in the LH), and between
463 response intensities recorded in this and previous studies (OSNs(45) or PNs(19)). A Fisher test, giving
464 a z value, was used to test the significance of the linear regression following Pearson correlation (R
465 package *multilevel*, *cordif* function). Mantel tests were used to compare matrices containing the
466 Euclidian distances for the 120 possible odor-pair among 16 odorants, either between different

imaging studies, or between neural and behavioral measures (R package *ade4*, *mantel.rtest* function). To explore similarity relationships among odorants, hierarchical clustering using Ward's classification method was used (R package *stats*, *hclust* function). All tests were performed with GraphPadPrism V7.00 and R (www.r-project.org).

ACKNOWLEDGEMENTS

We thank Robin Parlow, Eva Theilenberg, Marion Müller-Borg and Virginie Larcher for technical assistance. We thank Sara Bariselli for her support with the egg injection and Amélie Cabirol for fruitful discussions. We thank the French Research National Agency (ANR to JCS, Project ANR-17-CE20-0003 Bee-O-Choc), the CNRS (JCS) and the University Paris-Saclay (JC and JCS), the DFG (Deutsche Forschungsgemeinschaft to MB) for funding.

AUTHOR CONTRIBUTIONS

J.C., M.O., A.H., J.C.S., and M.B. conceived the experiments. J.C. and M.O. collected the data. J.C., M.O., A.H., J.C.S., and M.B. analysed the data and interpreted the results. J.C., A.H., J.C.S., and M.B. wrote the manuscript. All authors read and approved the final version of the manuscript.

COMPETING INTEREST STATEMENT

The present research project was conducted in the absence of any commercial relationships that could be construed as a potential conflict of interest.

488 **FIGURE LEGENDS**

489

490 **Figure 1: Genetically encoded GCaMP6f and its neural expression**

491 **A-** Scheme of the honey bee *synapsin* promoter *GCaMP6f* expression cassette. CDS: coding sequence;
492 UTR: untranslated region; ATG: translation start. **B-** GCaMP6f expression in the honey bee brain
493 revealed by anti-GFP immunostaining (left, in green). GCaMP6f is widely expressed in the bee brain,
494 including in somata and neural tracts (white arrows). For comparison with *synapsin* expression, an anti-
495 SYNORF1 immunostaining (right, in red) was also performed. Scale bar=200 µm **C-** GCaMP6f expression
496 (anti-GFP in green) and *synapsin* expression (anti-SYNORF1 in red) in the AL (left) and in the mushroom
497 bodies (right). Remarkable and strong expression is observed in the somata of projection neurons and
498 local neurons (near the AL) and in some somata of Kenyon cells (in the cup of the calyces). Scale bar=50
499 µm. AL: Antennal Lobe, MB: Mushroom body, OL: Optic Lobe, Lo: Lobulla, Me: Medulla, vL: vertical
500 lobe, lc: lateral cluster of projection neurons somata, mc: medial cluster of projection neurons somata,
501 Li: Lip, BR: Basal Ring, Co: Collar.

502

503 **Figure 2: Neural activity in the whole brain of the honey bee**

504 **A-** Hymenopteran olfactory pathway (adapted from (45)). Odorant molecules are detected by olfactory
505 sensory neurons (OSNs) on the antenna, which send olfactory information to the antennal lobe (AL).
506 Then, projection neurons (PNs) convey information to higher-order centers, the mushroom body (MB)
507 and the lateral horn (LH). Lo: lobula, Me: medulla, v: vertical lobe, h: horizontal lobe. **B-** Calcium signals
508 in the whole brain evoked by 3 different odorants (2-heptanone, octanal, heptanal) and the air control.
509 Relative fluorescence changes ($\Delta F/F$ [%]) are presented in a false-color code, from dark blue (minimal
510 response) to red (maximal response). **C-** Time course of odor-evoked responses ($\Delta F/F$ [%]) for one
511 individual to the presentation of 2-heptanone (in blue), octanal (in pink), and the air control (in grey),
512 simultaneously recorded in the AL (left), the LH (middle) and the MB (right). The calcium signals show
513 a biphasic time course, with a fluorescence increase upon odorant presentation (blue bars) followed

514 by a long-lasting fluorescence undershoot, in all brain regions.

515

516 **Figure 3: Neural activity recorded in the antennal lobe (AL)**

517 **A-** GCaMP6f calcium signals in the antennal lobe evoked by a panel of 16 odorants varying
518 systematically according to their carbon chain length (C6–C9) and their functional group (primary and
519 secondary alcohols, aldehydes, and ketones). Different odorants induce different glomerular activity
520 patterns. **B-** Time course of odor-evoked responses ($\Delta F/F$ [%]) recorded in the AL (in white squares
521 shown in A) to 2-heptanone (in blue), octanal (in pink), and to the air control (in grey). **C-** Amplitude of
522 calcium responses ($\Delta F/F$ [%]) to the 16 aliphatic odorants and to the air control. All odorants induce
523 significant activity in comparison to the air control (n = 11, ** $p < 0.0097$). **D-** Amplitude of calcium
524 responses ($\Delta F/F$ [%]) as a function of odorant vapor pressure (in log units). The linear regression shows
525 a significant correlation (R^2 = 0.84, *** p = 6e-7). **E-** Different presentations of the same odorants (2-
526 octanone and heptanal) show similar glomerular patterns in the AL (left). Dissimilarity measures
527 (Euclidian distance) between representations of the same or of different odorants. Activity maps are
528 more similar (shorter distances) when the same odorant is presented (*** p = 1.1e-4), showing, as
529 expected, a clear odor coding in this structure. **F-** Cluster analysis showing similarity relationships
530 among odorants (Ward's classification method). Functional groups are shown in different colors:
531 primary alcohols in blue, secondary alcohols in green, aldehydes in black, and ketones in red. The
532 analysis shows a first separation between odorants with short and long carbon chain lengths. Odorants
533 with a short carbon chain are then subdivided into alcohols (primary and secondary, C-OH functional
534 group) and ketones/aldehydes (C=O functional group).

535

536 **Figure 4: Neural activity recorded in the lateral horn (LH)**

537 **A-** Calcium signals in the lateral horn evoked by the same panel of 16 odorants. Different odorants
538 induce different activity patterns in the LH. **B-** Time course of odor-evoked responses ($\Delta F/F$ [%])
539 recorded in the LH (in white squares shown in A) to 2-heptanone (in blue), octanal (in pink), and to the

air control (in grey). The calcium signals also show a biphasic response, with a fluorescence increase upon odor presentation (blue bar) followed by a long undershoot. **C-** Amplitude of calcium responses ($\Delta F/F$ [%]) to the 16 aliphatic odorants and to the air control. All odorants induce a significant activity in comparison to the air control (n = 8, * $p < 0.04$). **D-** Cluster analysis showing similarity relationships among odorants (Ward's classification method).

Figure 5: Neural activity recorded in the mushroom bodies (MB)

A- Calcium signals in the calyces of the mushroom bodies in response to the presentations of 2-heptanone, heptanal, octanal, and the air control. **B-** Time course of odor-evoked responses ($\Delta F/F$ [%]) recorded in the lip of the MB (white squares shown in A) to 2-heptanone (in blue), octanal (in pink), and to the air control (in grey). Calcium signals are weaker here than in other structures, with a smaller first component and a larger second component. **C-** Amplitude of calcium responses ($\Delta F/F$ [%]) to the 5 tested odorants and to the air control. All odorants induce significant activity in comparison to the air control (n = 6, * $p < 0.05$, except 2-heptanone with p =0.07).

Supplementary Figure 1: Correlation between amplitudes of calcium responses recorded in the AL

A- Amplitude of calcium responses ($\Delta F/F$ [%]) recorded in Olfactory Sensory Neurons (OSNs) in(45) as a function of amplitude of calcium responses ($\Delta F/F$ [%]) recorded in the AL in this study. The linear regression shows a significant correlation (R^2 = 0.84, *** p = 6e-7). **B-** Amplitude of calcium responses ($\Delta F/F$ [%]) recorded in Projection Neurons (PNs) in(19) as a function of amplitude of calcium responses ($\Delta F/F$ [%]) recorded in the AL in this study. The linear regression shows a significant correlation (R^2 = 0.78, *** p = 6e-6).

Supplementary Figure 2: Synapsin sequence of the honey bee

The promoter and the 5' UTR sequence from the honey bee synapsin (syn) gene. Different colors indicate the different exons that were fused.

566 **REFERENCES**

567 1. Bourke AF (2011) *Principles of social evolution* (Oxford University Press).
568 2. Hamilton WD (1964) The genetical evolution of social behaviour. II. *Journal of theoretical*
569 *biology* 7(1):17-52.
570 3. Hölldobler B & Wilson EO (1990) *The ants* (Harvard University Press) pp 1-732.
571 4. Wilson EO (2012) *The social conquest of earth* (WW Norton & Company).
572 5. Oster GF & Wilson EO (1978) Caste and ecology in the social insects. *Monogr Popul Biol* 12:1-
573 352.
574 6. Paoli M & Galizia GC (2021) Olfactory coding in honeybees. *Cell and Tissue Research*:1-24.
575 7. Woodgate JL*, et al.* (2021) Harmonic radar tracking reveals that honeybee drones navigate
576 between multiple aerial leks. *iScience* 24(6):102499.
577 8. Avargues-Weber A, Dyer AG, Combe M, & Giurfa M (2012) Simultaneous mastering of two
578 abstract concepts by the miniature brain of bees. *Proc Natl Acad Sci U S A* 109(19):7481-7486.
579 9. Chole H*, et al.* (2019) Social Contact Acts as Appetitive Reinforcement and Supports Associative
580 Learning in Honeybees. *Curr Biol* 29(8):1407-1413 e1403.
581 10. Barron AB & Plath JA (2017) The evolution of honey bee dance communication: a mechanistic
582 perspective. *J Exp Biol* 220(Pt 23):4339-4346.
583 11. Giurfa M & Sandoz JC (2012) Invertebrate learning and memory: Fifty years of olfactory
584 conditioning of the proboscis extension response in honeybees. *Learn Mem* 19(2):54-66.
585 12. Wycke MA, Coureaud G, Thomas-Danguin T, & Sandoz JC (2020) Configural perception of a
586 binary olfactory mixture in honey bees, as in humans, rodents and newborn rabbits. *J Exp Biol*
587 223(Pt 21).
588 13. Paoli M*, et al.* (2018) Neuronal Response Latencies Encode First Odor Identity Information
589 across Subjects. *J Neurosci* 38(43):9240-9251.
590 14. Farris SM (2016) Insect societies and the social brain. *Curr Opin Insect Sci* 15:1-8.
591 15. Lihoreau M, Latty T, & Chittka L (2012) An exploration of the social brain hypothesis in insects.
592 *Front Physiol* 3:442.
593 16. Cabirol A, Brooks R, Groh C, Barron AB, & Devaud JM (2017) Experience during early adulthood
594 shapes the learning capacities and the number of synaptic boutons in the mushroom bodies
595 of honey bees (Apis mellifera). *Learn Mem* 24(10):557-562.
596 17. Suenami S, Iino S, & Kubo T (2018) Pharmacologic inhibition of phospholipase C in the brain
597 attenuates early memory formation in the honeybee (Apis mellifera L.). *Biol Open* 7(1).
598 18. Duer A, Paffhausen BH, & Menzel R (2015) High order neural correlates of social behavior in
599 the honeybee brain. *J Neurosci Methods* 254:1-9.
600 19. Carcaud J, Giurfa M, & Sandoz JC (2018) Differential Processing by Two Olfactory Subsystems
601 in the Honeybee Brain. *Neuroscience* 374:33-48.
602 20. Sherer LM & Certel SJ (2019) The fight to understand fighting: neurogenetic approaches to the
603 study of aggression in insects. *Current opinion in insect science* 36:18-24.
604 21. McKelvey EG & Fabre CC (2019) Recent neurogenetic findings in insect courtship behaviour.
605 *Current opinion in insect science* 36:103-110.
606 22. Ehmann N & Pauls D (2020) Optogenetics: illuminating neuronal circuits of memory formation.
607 *Journal of neurogenetics* 34(1):47-54.
608 23. Sadanandappa MK, Sathyanarayana SH, Kondo S, & Bosco G (2021) Neuropeptide F signaling
609 regulates parasitoid-specific germline development and egg-laying in Drosophila. *PLoS*
610 *genetics* 17(3):e1009456.
611 24. Pooryasin A*, et al.* (2021) Unc13A and Unc13B contribute to the decoding of distinct sensory
612 information in Drosophila. *Nature Communications* 12(1):1-14.
613 25. Grover D, Katsuki T, Li J, Dawkins TJ, & Greenspan RJ (2020) Imaging brain activity during
614 complex social behaviors in Drosophila with Flyception2. *Nature communications* 11(1):1-10.
615 26. Jové V*, et al.* (2020) Sensory discrimination of blood and floral nectar by aedes aegypti
616 mosquitoes. *Neuron*.

27. Vinauger C*, et al.* (2019) Visual-olfactory integration in the human disease vector mosquito Aedes aegypti. *Current Biology* 29(15):2509-2516. e2505.
28. Koutroumpa FA*, et al.* (2016) Heritable genome editing with CRISPR/Cas9 induces anosmia in a crop pest moth. *Sci Rep* 6:29620.
29. Fandino RA*, et al.* (2019) Mutagenesis of odorant coreceptor Orco fully disrupts foraging but not oviposition behaviors in the hawkmoth Manduca sexta. *Proceedings of the National Academy of Sciences* 116(31):15677-15685.
30. DeGennaro M*, et al.* (2013) orco mutant mosquitoes lose strong preference for humans and are not repelled by volatile DEET. *Nature* 498(7455):487-491.
31. McMeniman CJ, Corfas RA, Matthews BJ, Ritchie SA, & Vosshall LB (2014) Multimodal integration of carbon dioxide and other sensory cues drives mosquito attraction to humans. *Cell* 156(5):1060-1071.
32. Zhang ZJ*, et al.* (2019) A determining factor for insect feeding preference in the silkworm, Bombyx mori. *PLoS Biol* 17(2):e3000162.
33. Schulte C, Theilenberg E, Muller-Borg M, Gempe T, & Beye M (2014) Highly efficient integration and expression of piggyBac-derived cassettes in the honeybee (Apis mellifera). *Proc Natl Acad Sci U S A* 111(24):9003-9008.
34. Roth A*, et al.* (2019) A genetic switch for worker nutrition-mediated traits in honeybees. *PLoS biology* 17(3):e3000171.
35. Chen Z*, et al.* (2021) Neurodevelopmental and transcriptomic effects of CRISPR/Cas9-induced somatic orco mutation in honey bees. *Journal of Neurogenetics*:1-13.
36. Değirmenci L*, et al.* (2020) CRISPR/Cas 9-mediated mutations as a new tool for studying taste in honeybees. *Chemical Senses* 45(8):655-666.
37. Nie H-Y*, et al.* (2021) CRISPR/Cas9 mediated knockout of Amyellow-y gene results in melanization defect of the cuticle in adult Apis mellifera. *Journal of Insect Physiology* 132:104264.
38. Wang JW, Wong AM, Flores J, Vosshall LB, & Axel R (2003) Two-photon calcium imaging reveals an odor-evoked map of activity in the fly brain. *Cell* 112(2):271-282.
39. Muto A*, et al.* (2011) Genetic visualization with an improved GCaMP calcium indicator reveals spatiotemporal activation of the spinal motor neurons in zebrafish. *Proc Natl Acad Sci U S A* 108(13):5425-5430.
40. Chen TW*, et al.* (2013) Ultrasensitive fluorescent proteins for imaging neuronal activity. *Nature* 499(7458):295-300.
41. Otte M*, et al.* (2018) Improving genetic transformation rates in honeybees. *Sci Rep* 8(1):16534.
42. Strausfeld NJ (2002) Organization of the honey bee mushroom body: representation of the calyx within the vertical and gamma lobes. *J Comp Neurol.* 450(1):4-33.
43. Suenami S, Oya S, Kohno H, & Kubo T (2018) Kenyon Cell Subtypes/Populations in the Honeybee Mushroom Bodies: Possible Function Based on Their Gene Expression Profiles, Differentiation, Possible Evolution, and Application of Genome Editing. *Front Psychol* 9:1717.
44. Joerges J, Küttner A, Galizia CG, & Menzel R (1997) Representations of odours and odour mixtures visualized in the honeybee brain. *Nature* 387:285-288.
45. Carcaud J, Hill T, Giurfa M, & Sandoz JC (2012) Differential coding by two olfactory subsystems in the honeybee brain. *J Neurophysiol* 108(4):1106-1121.
46. Galizia CG, Nägler K, Hölldobler B, & Menzel R (1998) Odour coding is bilaterally symmetrical in the antennal lobe of honeybees (Apis mellifera). *European Journal of Neuroscience* 10:2964-2974.
47. Sachse S & Galizia CG (2002) The role of inhibition for temporal and spatial odor representation in olfactory output neurons: a calcium imaging study. *Journal of Neurophysiology* 87:1106-1117.
48. Guerrieri F, Schubert M, Sandoz JC, & Giurfa M (2005) Perceptual and neural olfactory similarity in honeybees. *PLoS Biology* 3(4):e60.

49. Lin MZ & Schnitzer MJ (2016) Genetically encoded indicators of neuronal activity. *Nat Neurosci* 19(9):1142-1153.
50. Dana H*, et al.* (2019) High-performance calcium sensors for imaging activity in neuronal populations and microcompartments. *Nat Methods* 16(7):649-657.
51. Groh C, Lu Z, Meinertzhagen IA, & Rössler W (2012) Age-related plasticity in the synaptic ultrastructure of neurons in the mushroom body calyx of the adult honeybee Apis mellifera. *J Comp Neurol* 520(15):3509-3527.
52. Suenami S, Oya S, Kohno H, & Kubo T (2018) Kenyon cell subtypes/populations in the honeybee mushroom bodies: possible function based on their gene expression profiles, differentiation, possible evolution, and application of genome editing. *Frontiers in psychology* 9:1717.
53. Sachse S, Rappert A, & Galizia CG (1999) The Spatial representation of chemical structures in the antennal lobe of honeybees: steps towards the olfactory code. *European Journal of Neuroscience* 11:3970-3982.
54. Roussel E, Carcaud J, Combe M, Giurfa M, & Sandoz JC (2014) Olfactory coding in the honeybee lateral horn. *Curr Biol* 24(5):561-567.
55. Strutz A*, et al.* (2014) Decoding odor quality and intensity in the Drosophila brain. *eLife* 3:e04147.
56. Dolan MJ*, et al.* (2019) Neurogenetic dissection of the Drosophila lateral horn reveals major outputs, diverse behavioural functions, and interactions with the mushroom body. *eLife* 8.
57. Faber T & Menzel R (2001) Visualizing mushroom body response to a conditioned odor in honeybees. *Naturwissenschaften* 88(11):472-476.
58. Szyszka P, Ditzen M, Galkin A, Galizia CG, & Menzel R (2005) Sparsening and temporal sharpening of olfactory representations in the honeybee mushroom bodies. *J.Neurophysiol.* 94(5):3303-3313.
59. Paoli M & Haase A (2018) In Vivo Two-Photon Imaging of the Olfactory System in Insects. *Methods in molecular biology* 1820:179-219.
60. Bilz F, Geurten BRH, Hancock CE, Widmann A, & Fiala A (2020) Visualization of a Distributed Synaptic Memory Code in the Drosophila Brain. *Neuron* 106(6):963-976 e964.
61. Ai H, Kai K, Kumaraswamy A, Ikeno H, & Wachtler T (2017) Interneurons in the Honeybee Primary Auditory Center Responding to Waggle Dance-Like Vibration Pulses. *J Neurosci* 37(44):10624-10635.
62. Tiraboschi E, Leonardelli L, Segata G, Rigosi E, & Haase A (2021) Parallel processing of olfactory and mechanosensory information in the honeybee antennal lobe. *bioRxiv*:2021.2005.2011.443598.
63. Groh C & Rössler W (2020) Analysis of synaptic microcircuits in the mushroom bodies of the honeybee. *Insects* 11(1):43.
64. Ott SR (2008) Confocal microscopy in large insect brains: zinc-formaldehyde fixation improves synapsin immunostaining and preservation of morphology in whole-mounts. *J Neurosci Methods* 172(2):220-230.
65. Carcaud J, Giurfa M, & Sandoz JC (2015) Differential combinatorial coding of pheromones in two olfactory subsystems of the honey bee brain. *J Neurosci* 35(10):4157-4167.

Figure 1

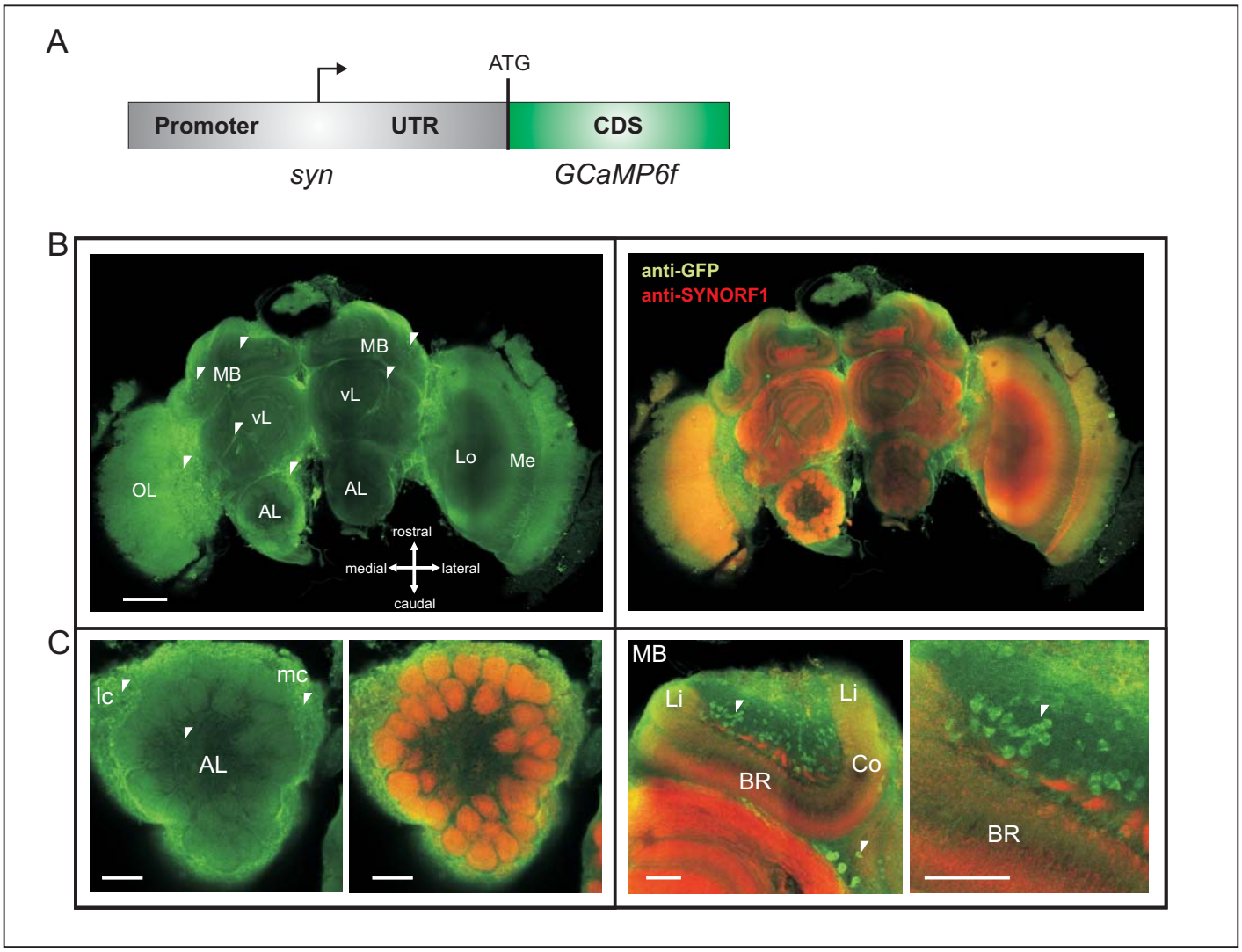

Figure 1: Genetically encoded GCaMP6f and its neural expression

A- Scheme of the honey bee *synapsin* promoter *GCaMP6f* expression cassette. CDS: coding sequence; UTR: untranslated region; ATG: translation start. **B-** GCaMP6f expression in the honey bee brain revealed by anti-GFP immunostaining (left, in green). GCaMP6f is widely expressed in the bee brain, including in somata and neural tracts (white arrows). For comparison with *synapsin* expression, an anti-SYNORF1 immunostaining (right, in red) was also performed. Scale bar=200 µm **C-** GCaMP6f expression (anti-GFP in green) and *synapsin* expression (anti-SYNORF1 in red) in the AL (left) and in the mushroom bodies (right). Remarkable and strong expression is observed in the somata of projection neurons and local neurons (near the AL) and in some somata of Kenyon cells (in the cup of the calyces). Scale bar=50 µm. AL: Antennal Lobe, MB: Mushroom body, OL: Optic Lobe, Lo: Lobulla, Me: Medulla, vL: vertical lobe, lc: lateral cluster of projection neurons somata, mc: medial cluster of projection neurons somata, Li: Lip, BR: Basal Ring, Co: Collar.

Figure 2

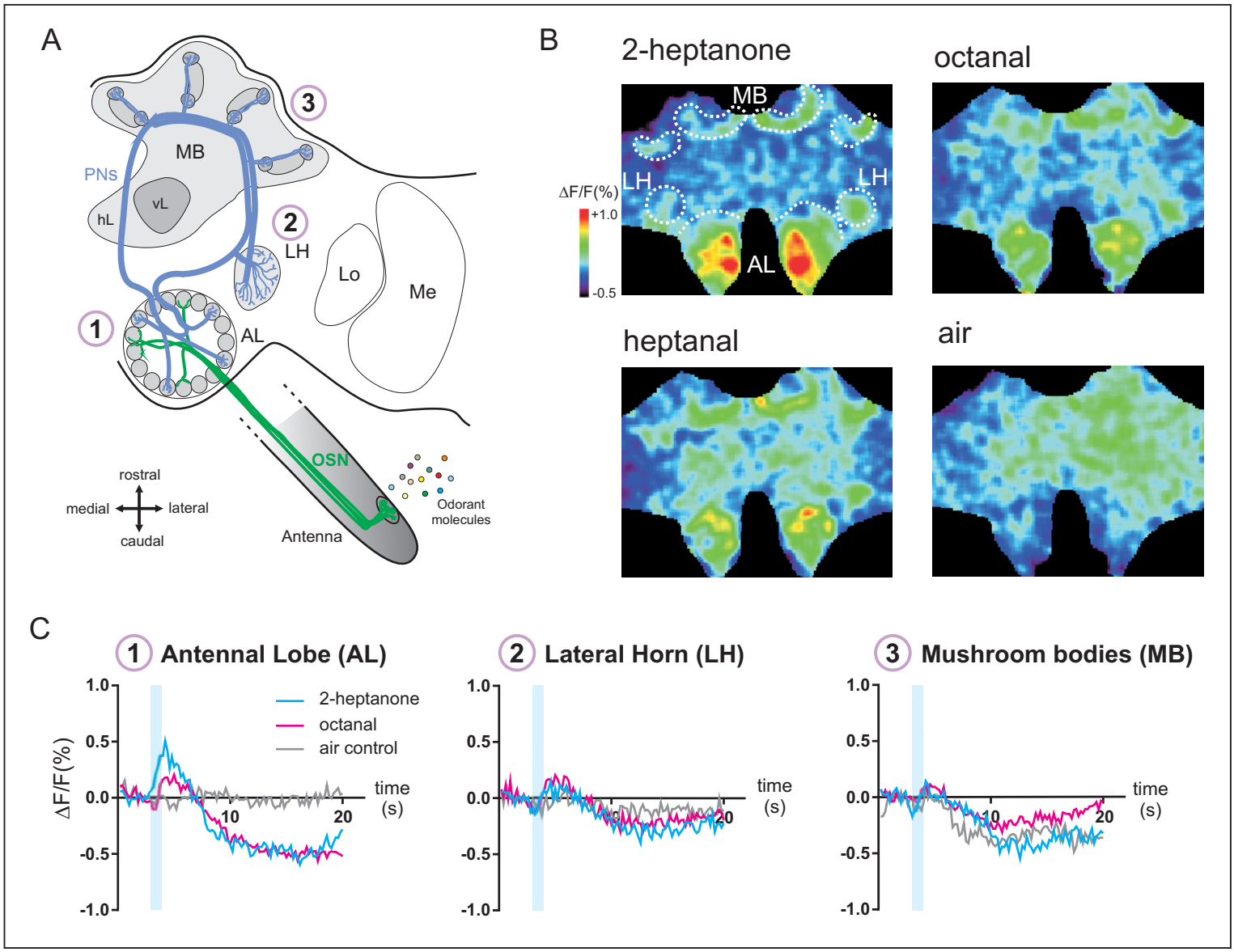

Figure 2: Neural activity in the whole brain of the honey bee

A- Hymenopteran olfactory pathway (adapted from [40]). Odorant molecules are detected by olfactory sensory neurons (OSNs) on the antenna, which send olfactory information to the antennal lobe (AL). Then, projection neurons (PNs) convey information to higher-order centers, the mushroom body (MB) and the lateral horn (LH). Lo: lobula, Me: medulla, v: vertical lobe, h: horizontal lobe. **B-** Calcium signals in the whole brain evoked by 3 different odorants (2-heptanone, octanal, heptanal) and the air control. Relative fluorescence changes ($\Delta F/F$ [%]) are presented in a false-color code, from dark blue (minimal response) to red (maximal response). **C-** Time course of odor-evoked responses ($\Delta F/F$ [%]) for one individual to the presentation of 2-heptanone (in blue), octanal (in pink), and the air control (in grey), simultaneously recorded in the AL (left), the LH (middle) and the MB (right). The calcium signals show a biphasic time course, with a fluorescence increase upon odorant presentation (blue bars) followed by a long-lasting fluorescence undershoot, in all brain regions.

Figure 3

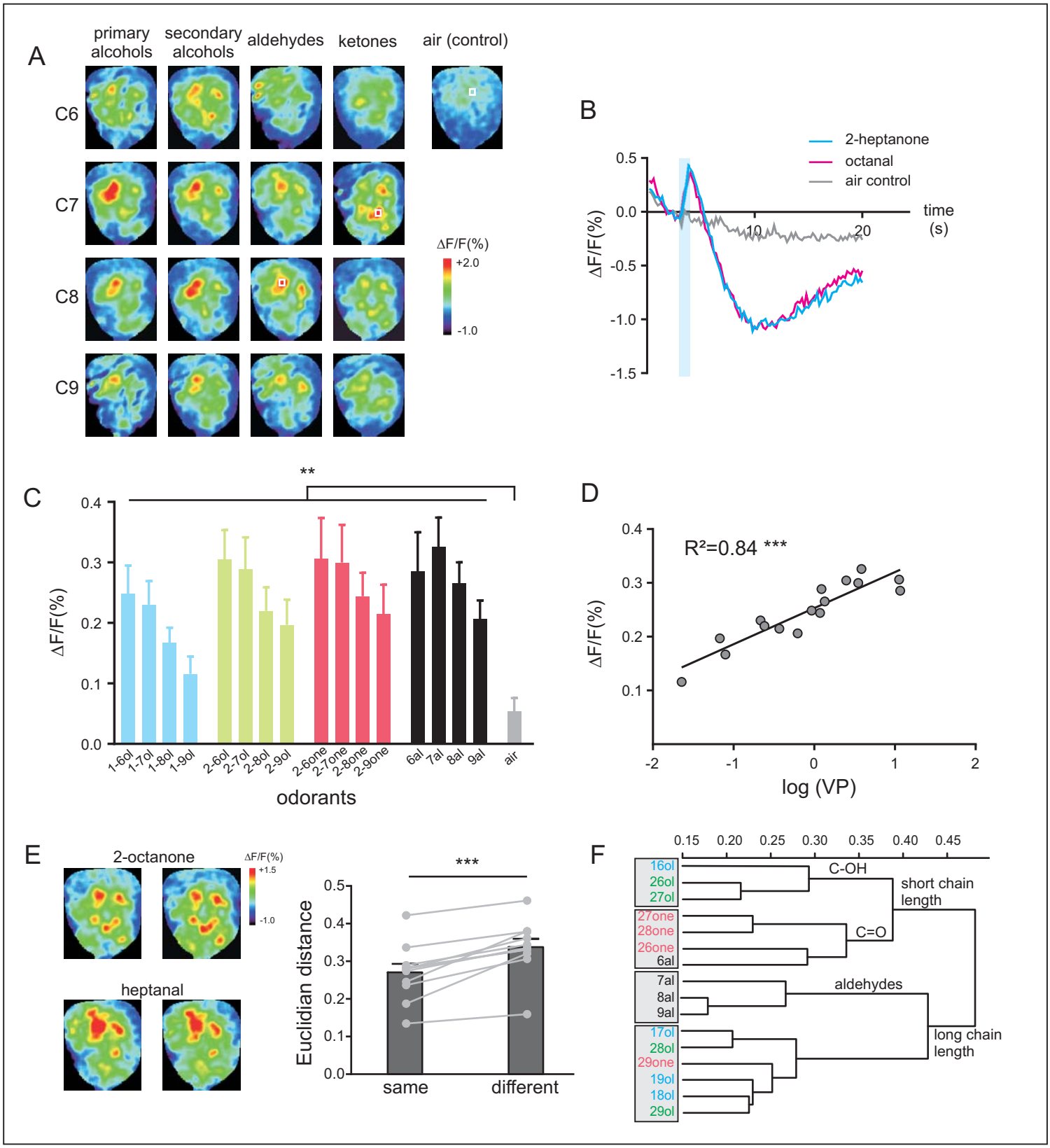

Figure 3: Neural activity recorded in the antennal lobe (AL)

A- GCaMP6f calcium signals in the antennal lobe evoked by a panel of 16 odorants varying systematically according to their carbon chain length (C6–C9) and their functional group (primary and secondary alcohols, aldehydes, and ketones). Different odorants induce different glomerular activity patterns. **B-** Time course of odor-evoked responses ($\Delta F/F$ [%]) recorded in the AL (in white squares shown in A) to 2-heptanone (in blue), octanal (in pink), and to the air control (in grey). **C-** Amplitude of calcium responses ($\Delta F/F$ [%]) to the 16 aliphatic odorants and to the air control. All odorants induce significant activity in comparison to the air control (n = 11, ** $p < 0.0097$). **D-** Amplitude of calcium responses ($\Delta F/F$ [%]) as a function of odorant vapor pressure (in log units). The linear regression shows a significant correlation (R^2 = 0.84, *** p = 6e-7). **E-** Different presentations of the same odorants (2-octanone and heptanal) show similar glomerular patterns in the AL (left). Dissimilarity measures (Euclidian distance) between representations of the same or of different odorants. Activity maps are more similar (shorter distances) when the same odorant is presented (*** p = 1.1e-4), showing, as expected, a clear odor coding in this structure. **F-** Cluster analysis showing similarity relationships among odorants (Ward's classification method). Functional groups are shown in different colors: primary alcohols in blue, secondary alcohols in green, aldehydes in black, and ketones in red. The analysis shows a first separation between odorants with short and long carbon chain lengths. Odorants with a short carbon chain are then subdivided into alcohols (primary and secondary, C-OH functional group) and ketones/aldehydes (C=O functional group).

Figure 4

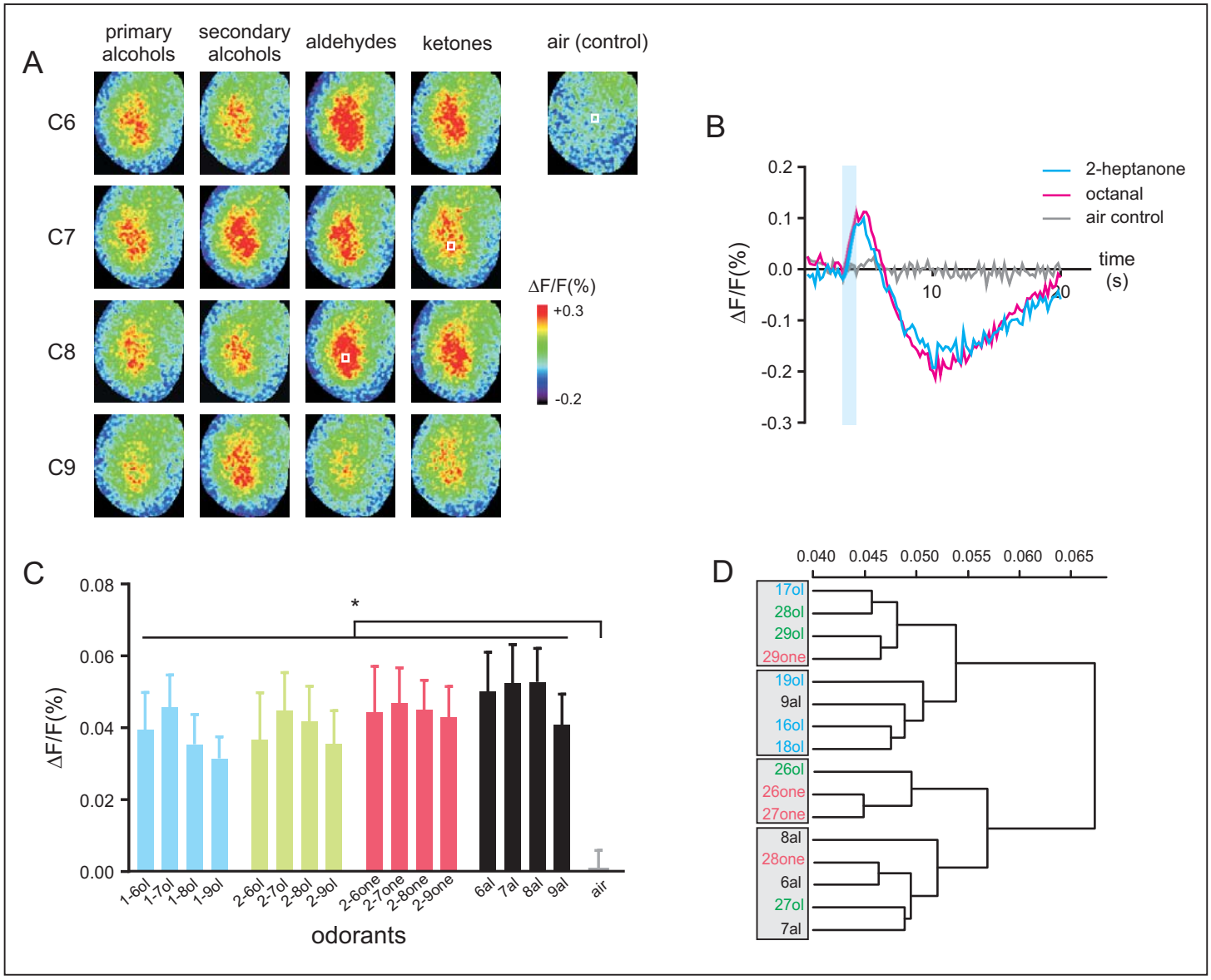

Figure 4: Neural activity recorded in the lateral horn (LH)

A- Calcium signals in the lateral horn evoked by the same panel of 16 odorants. Different odorants induce different activity patterns in the LH. **B-** Time course of odor-evoked responses ($\Delta F/F$ [%]) recorded in the LH (in white squares shown in A) to 2-heptanone (in blue), octanal (in pink), and to the air control (in grey). The calcium signals also show a biphasic response, with a fluorescence increase upon odor presentation (blue bar) followed by a long undershoot. **C-** Amplitude of calcium responses ($\Delta F/F$ [%]) to the 16 aliphatic odorants and to the air control. All odorants induce a significant activity in comparison to the air control ($n = 8$, * $p < 0.04$). **D-** Cluster analysis showing similarity relationships among odorants (Ward's classification method).

Figure 5

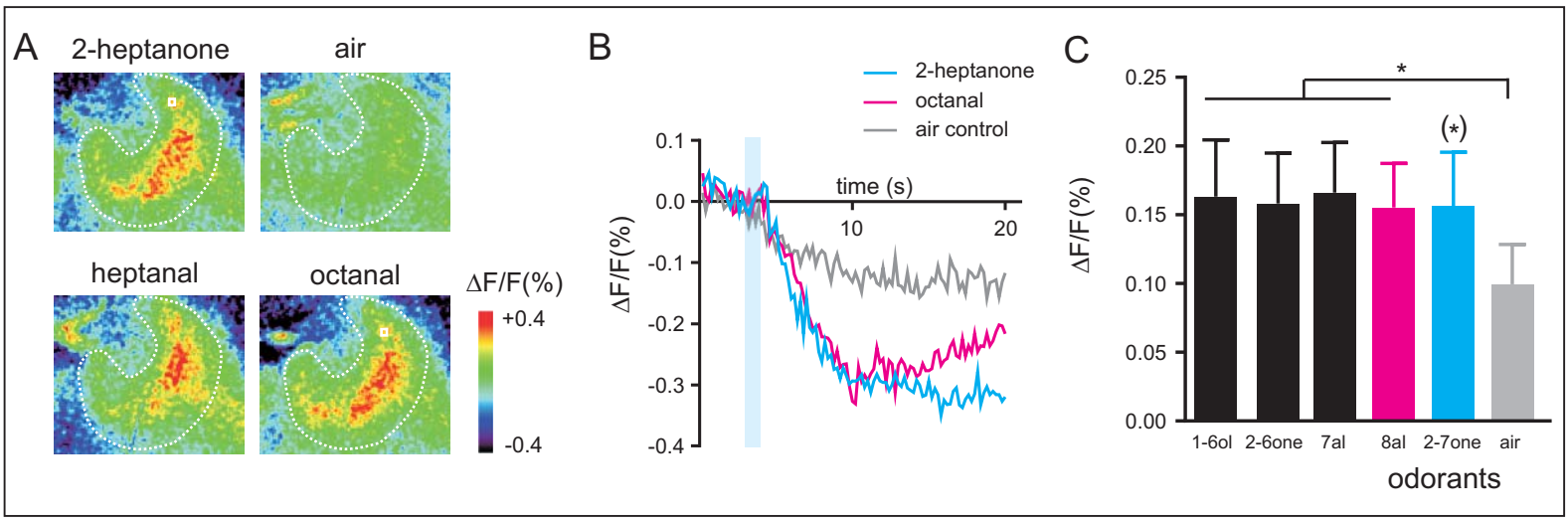

Figure 5: Neural activity recorded in the mushroom bodies (MB)
A- Calcium signals in the calyces of the mushroom bodies in response to the presentations of 2-heptanone, heptanal, octanal, and the air control. **B-** Time course of odor-evoked responses ($\Delta F/F$ [%]) recorded in the lip of the MB (white squares shown in A) to 2-heptanone (in blue), octanal (in pink), and to the air control (in grey). Calcium signals are weaker here than in other structures, with a smaller first component and a larger second component. **C-** Amplitude of calcium responses ($\Delta F/F$ [%]) to the 5 tested odorants and to the air control. All odorants induce significant activity in comparison to the air control (n = 6, * $p < 0.05$, except 2-heptanone with p =0.07).

Sup. Figure 1

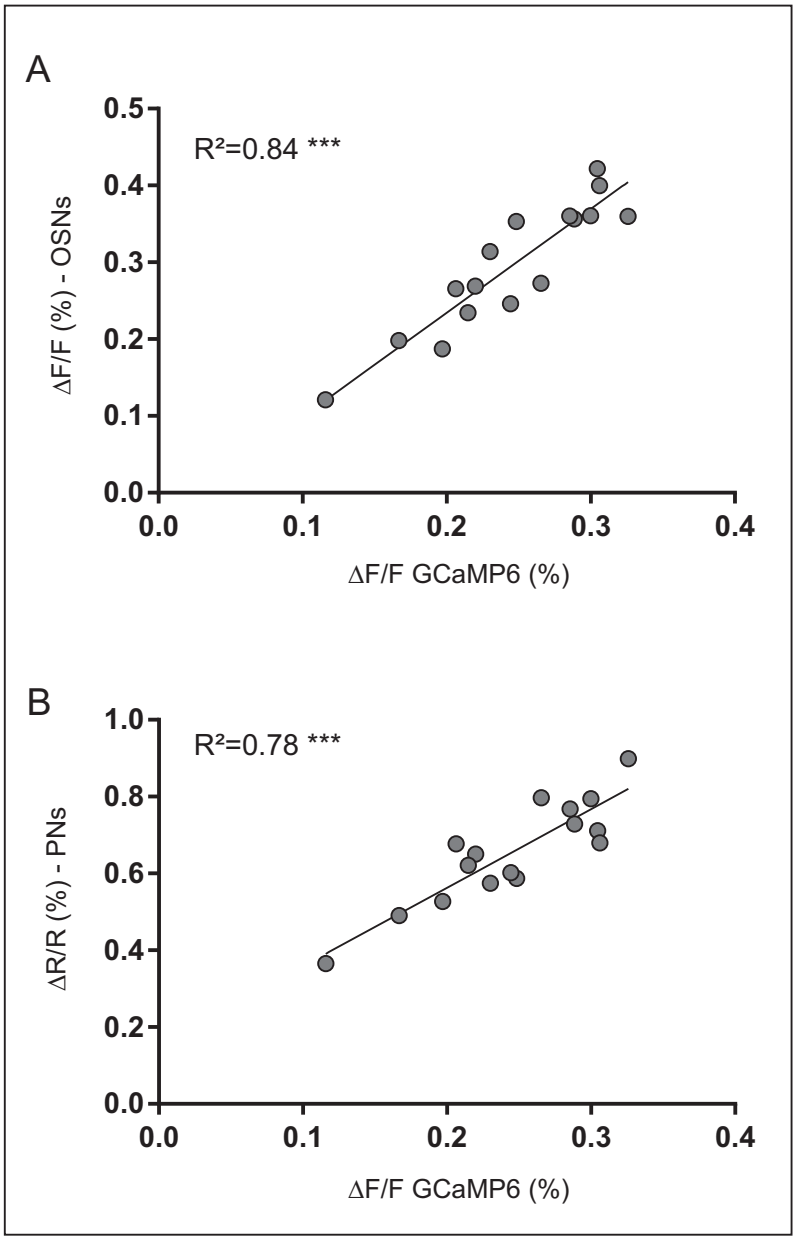

Supplementary Figure 1: Correlation between amplitudes of calcium responses recorded in the AL
A- Amplitude of calcium responses (Δ*F*/*F* [%]) recorded in Olfactory Sensory Neurons (OSNs) in[40] as a function of amplitude of calcium responses (Δ*F*/*F* [%]) recorded in the AL in this study. The linear regression shows a significant correlation (R^2 = 0.84, *** p = 6e-7). **B-** Amplitude of calcium responses (Δ*F*/*F* [%]) recorded in Projection Neurons (PNs) in[26] as a function of amplitude of calcium responses (Δ*F*/*F* [%]) recorded in the AL in this study. The linear regression shows a significant correlation (R^2 = 0.78, *** p = 6e-6).

ACGAGAACCGGGAAGCGTAGTGATAATCTTAATGAAAATCCCCCACGTTCGTGCCTCCTTTGATAGTTTTCACC
CCGGGAAAATGTTTGTGACCCACTTTTCCCACAGAAAACGCTCTAATGCCGTTTTACCTGGGGTGCAAAAAGGT
AGAGTGGGGAAAAAAAAAAAAAAAAGAGGCGGAACCGGAGGAGAGAAGAGAAGAGAGAACCCCGTCTTCT
ACTTGAATACCGTGTCTCGCGCCGTATACGCAAACGTGTACAATATATATAACAATTTTATTGCAAGAATTTCAA
ACAACGCTACGGAGATCAAGGGATCATATAAGAATTTTTATACGTCCTTACAACAGGAAAATTCGTTCCCAAGA
TTCCACGAGTTGTAACGCATGCTGTCTAACCGCACGCATACACACGCACCCCGATACACAATAGAGAAACTCTC
TCTCCTCTCTCTCTCTCTCCCGAAACCGTTTCAAAAATGTACGATCTCCGTAAGATCGTACAAAAGCTCGGGAAT
AAATGCAACGACGAGGAATCACGAATAACTGGGTCGCTGCATTAATTCTTTTATCCAGGCCGACTTATCCGTGG
AGAATGGCGGTCGAGTGGCGAGCAACGAGAAGAATCAACATCATCCATCCGGCACACTCTCTCTATAATTATC
GCGATATCGAAGGAAGGGAAAAAGCGAGGAGTAGAATTTCGAGTTGCAAAGAGATAATATTATATCCCGTTT
CCCTTCCTCCTCCTATTAACTTTCAATCTCATTGCGAACCTCCAGTTTCCTCCAATTTTATATAATATTTTGAAAAG
AGGCGGCTATGCAGAGAATAGAAAAGAAAAAAAAAAGAAAAAGAAGAAATCAGAAGCGCATGCAAACGCGT
TTACCAATGAGCGGGCCGACGTTTCGTCTTCGGTTCGGCCAGCAGGTGGAGCGTGTTTGATGTGAATCGAACA
ACGTCACCCTGTACAAACACCGGGGACCGGGCAGCATATAGGGGCTCGTCCTTTTTTTCCCCGTCGTCGTCGTC
GTCGTTAGCTCGCGAGACTGGGTGAGGAGGGGGTGATAAGGAGGACGCAAGCGCGGACCTATCGACCAGCT
AACCCTCCGGGTAACACCCTCGCGATCCTCGGCCGAGGCTCACTGCTTCACCGGCAAACTAGTAGGTAGTACA
CGCACGCGACACAGATTTCAACTTGGATTGTTTAGTTTCTCCTTCCTCACCTCTCTTATTTCATCCTTTCCTTTCGG
ATTACCTTACGTTCAACTGTTATTCCACAAACTCGGCAAGGGAACGCAACATCTCGTTCGAACGCACATCGTCG
AGCGAAGAAGAGATCACGTCGGCGAGACGACGTCCTTTCCGGTAACCGCCGCGTTTACGAGAAAGGGACAGA
CAGAAGGGGGAGAGCGTAGCGGTGTCCACGCCAACGAAAACACCAACGAAGCGGAATTCTGCGGTTTTCGCG
AGGAGGGCGAGGTCGGTGTTAAACCAGCAAGATTACCGGCCGCGGCGGTTGCGCCAAATACTGTGGTACAGC
TACTTCACCCGGCAACATTTCATTCTCCAGCTTTCGACAGTCCTTCACCTCCAATGTTAACTACCTGAAACGGAG
GTTCTCGTCAGGGGATTTGAGCTCGGAGCTCGACGATGAACCAAGCACAGACTCCGGGCTGGCCTCCATG

Supplementary Figure 2: Synapsin sequence of the honey bee

The promoter and the 5’ UTR sequence from the honey bee synapsin (syn) gene. Different colors indicate the different exons that were fused.